ACS OMEGA

http://pubs.acs.org/journal/acsodf

Article

Conjugated Dienones from Differently Substituted Cinnamaldehyde as Highly Potent Monoamine Oxidase-B Inhibitors: Synthesis, Biochemistry, and Computational Chemistry

Bijo Mathew,*,▽ Jong Min Oh,▽ Mohamed A. Abdelgawad, Ahmed Khames, Mohammed M. Ghoneim, Sunil Kumar, Lekshmi R. Nath, Sachithra Thazhathuveedu Sudevan, Della Grace Thomas Parambi, Clement Agoni, Mahmoud E. S. Soliman, and Hoon Kim*

Cite This: *ACS Omega* 2022, 7, 8184−8197

Read Online

ACCESS | Metrics & More | Article Recommendations | Supporting Information

ABSTRACT: Fifteen multiconjugated dienones (**MK1**−**MK15**) were synthesized and evaluated to determine their inhibitory activities against monoamine oxidases (MAOs) A and B. All derivatives were found to be potent and highly selective MAO-B inhibitors. Compound **MK6**, with an IC_{50} value of 2.82 nM, most effectively inhibited MAO-B, like **MK12** (IC_{50} = 3.22 nM), followed by **MK5**, **MK13**, and **MK14** (IC_{50} = 4.02, 4.24, and 4.89 nM, respectively). The selectivity index values of **MK6** and **MK12** for MAO-B over MAO-A were 7361.5 and 1780.5, respectively. Compounds **MK6** and **MK12** were competitive reversible inhibitors of MAO-B, with K_i values of 1.10 ± 0.20 and 3.0 ± 0.27 nM, respectively. Cytotoxic studies showed that **MK5**, **MK6**, **MK12**, and **MK14** exhibited low toxicities on Vero cells, with IC_{50} values of 218.4, 149.1, 99.96, and 162.3 μg/mL, respectively, which were much higher than those for their effective nanomolar-level concentrations. Also, **MK5**, **MK6**, **MK12**, and **MK14** decreased cell damage in H_2O_2-induced cells via a significant scavenging effect of reactive oxygen species. Molecular modeling was performed to rationalize the potential inhibitory activities of **MK5**, **MK6**, **MK12**, and **MK14** toward MAO-B and their possible binding mechanisms, showing high-affinity binding pocket interactions and conformation perturbations of the compounds with MAO-B, which were interpreted as the conformational dynamics of MAO-B. This study concluded that all the compounds tested were more potent MAO-B inhibitors than the reference drugs, and leading compounds could be further explored for their effectiveness in various kinds of neurodegenerative disorders.

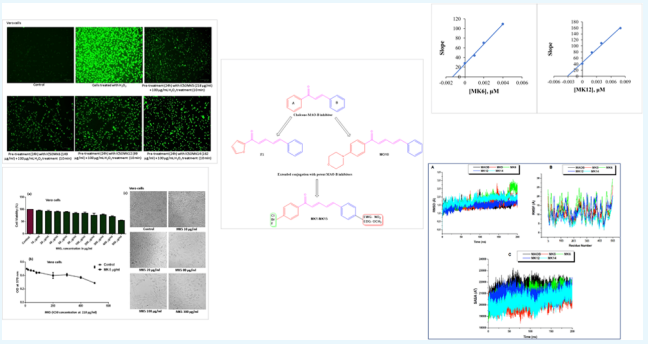

INTRODUCTION

Monoamine oxidases (MAOs) are the prime metabolizing enzymes of various biogenic amines via oxidative deamination.[1] The alteration of biogenic amine concentrations in the brain by MAO directly correlates with several neurological disorders, such as Parkinson's disease (PD) and Alzheimer's disease (AD).[2] This oxidative degradation generates toxic byproducts, such as hydrogen peroxide, reactive oxygen species (ROS), and ammonia, which can trigger oxidative stress with mitochondrial dysfunction in neural cells.[3,4] High levels of MAO-B have been observed in the substantia nigra of PD patients, and progressively reversible and highly selective MAO-B inhibitors have proved efficient for relieving the symptoms of PD patients.[5]

Chalcones are simple organic compounds with enone-based linkers between phenyl and hetero nuclei.[6] Numerous structural manipulations have been applied to the chalcone scaffold as a selective MAO-B inhibitor, changing the hetero nucleus by placing various electron-withdrawing and/or electron-donating groups on the two aromatic/heteroaromatic rings.[7] These studies have demonstrated that factors such as the length, electron delocalization, and hydrophobicity of rings around linkers play a crucial role in the development of MAO inhibitors.[8−15]

In 2013, Desideri et al. reported that an extended conjugation in the chalcone framework could exhibit remarkable MAO-B inhibition; compounds (2*E*,4*E*)-5-(4-chlorophenyl)-1-(2-hydroxy-4-methoxyphenyl)penta-2,4-dien-1-one and (2*E*,4*E*)-5-(4-chlorophenyl)-1-(2,4-dihydroxyphenyl)penta-2,4-dien-1-one were the most potent human MAO-B inhibitors, with IC_{50} values of 4.51 and 11.35

Received: January 19, 2022
Accepted: February 11, 2022
Published: February 24, 2022

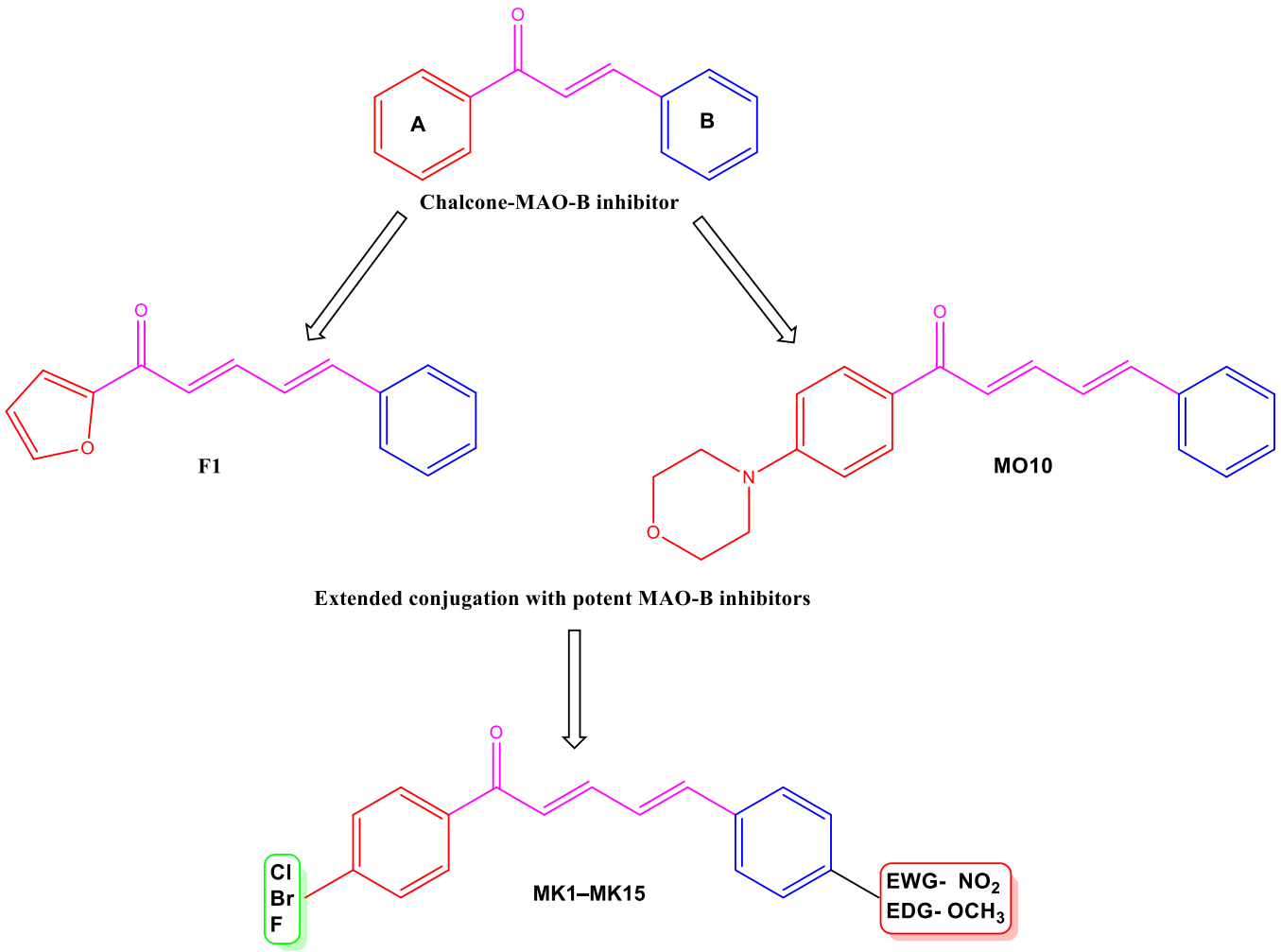

Figure 1. Design strategy for conjugated dienones as potent MAO-B inhibitors.

Scheme 1. Synthesis of Multiconjugated Ketones (MK1−MK15): (a) Pyrrolidine and (b) Ethanol

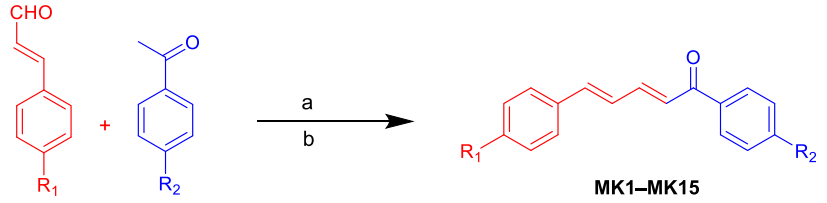

ID	R_1	R_2
MK1	H	Cl
MK2	Br	Cl
MK3	OCH_3	Cl
MK4	F	Cl
MK5	NO_2	Cl
MK6	H	Br
MK7	Br	Br
MK8	OCH_3	Br
MK9	F	Br
MK10	NO_2	Br
MK11	Br	F
MK12	OCH3	F
MK13	NO_2	F
MK14	OCH_3	H
MK15	NO_2	H

nM, respectively.[16] A previous research report from our laboratory showed that extended conjugations in chalcone linkers exhibited MAO-B inhibitory activity; an unsaturation extension on the furan-based chalcone (**F1**) improved the MAO-B inhibitory activity (K_i = 0.0041 μM) and, to a greater extent, the selectivity index (SI = 172.4).[17] The extended conjugation was also appraised in 1-[4-(morpholin-4-yl)-phenyl]-5-phenylpenta-2,4-dien-1-one (**MO10**) as a potent

https://doi.org/10.1021/acsomega.2c00397
ACS Omega 2022, 7, 8184−8197

Table 1. Inhibition of MAO-A, MAO-B, AChE, BChE, and BACE1 by the MK series[a]

	residual activity (%)					IC_{50} (μM, nM)		
	MAO-A	MAO-B	AChE	BChE	BACE1	MAO-A	MAO-B	
compounds	10 μM	1 μM	10 μM	10 μM	10 μM	(μM)	(nM)	SI[b]
MK1	83.0 ± 2.71	2.17 ± 1.49	84.0 ± 0.23	94.1 ± 4.72	77.1 ± 0.0087	16.7 ± 0.40	11.17 ± 1.65	1498.2
MK2	97.8 ± 0.16	14.3 ± 0.43	82.4 ± 0.98	95.4 ± 2.86	81.4 ± 0.97	23.5 ± 0.86	101.15 ± 1.63	232.4
MK3	73.6 ± 2.83	5.81 ± 0.27	81.4 ± 1.06	83.2 ± 0.46	84.8 ± 0.53	16.9 ± 0.50	13.07 ± 0.81	1290.2
MK4	77.0 ± 6.20	1.61 ± 2.28	90.7 ± 0.57	94.9 ± 7.16	72.5 ± 0.90	15.6 ± 0.63	9.67 ± 0.47	1609.8
MK5	72.9 ± 0.44	5.81 ± 0.27	74.1 ± 1.42	71.6 ± 1.05	73.3 ± 2.51	19.2 ± 0.94	4.02 ± 0.13	4783.0
MK6	84.0 ± 1.22	−1.69 ± 1.02	74.7 ± 0.66	97.5 ± 3.58	74.1 ± 1.48	20.6 ± 1.02	2.82 ± 0.39	7361.5
MK7	85.4 ± 1.99	8.90 ± 0.15	75.8 ± 0.73	99.2 ± 1.09	84.5 ± 0.91	21.7 ± 2.01	15.50 ± 0.06	1400.0
MK8	69.6 ± 2.03	7.85 ± 0.22	86.1 ± 5.10	80.7 ± 7.70	80.9 ± 1.67	24.1 ± 0.038	16.69 ± 0.62	1443.8
MK9	74.9 ± 1.29	2.60 ± 0.57	57.7 ± 0.00	87.4 ± 6.95	65.0 ± 1.61	22.5 ± 0.047	13.48 ± 1.06	1671.7
MK10	69.1 ± 1.32	3.40 ± 0.14	84.0 ± 0.73	87.9 ± 1.86	69.4 ± 1.03	19.5 ± 0.59	40.62 ± 0.87	481.0
MK11	76.9 ± 3.02	3.45 ± 0.21	77.8 ± 2.19	89.2 ± 6.58	71.4 ± 1.03	27.5 ± 0.82	19.75 ± 0.53	1394.7
MK12	40.9 ± 1.24	−2.71 ± 0.73	93.3 ± 0.73	94.6 ± 1.11	81.4 ± 1.03	5.70 ± 0.72	3.22 ± 0.04	1780.5
MK13	71.5 ± 8.06	1.95 ± 0.067	91.5 ± 0.80	97.8 ± 1.55	76.7 ± 0.64	23.7 ± 0.17	4.24 ± 0.13	5635.2
MK14	61.4 ± 6.27	−0.95 ± 1.35	84.7 ± 5.62	89.0 ± 1.55	77.3 ± 1.23	18.9 ± 1.02	4.89 ± 0.17	3871.5
MK15	54.4 ± 5.37	−3.52 ± 0.41	68.8 ± 0.80	80.2 ± 1.55	89.5 ± 0.92	12.7 ± 0.57	12.40 ± 7.92	1025.8
toloxatone						1.08 ± 0.025		
lazabemide							110.00 ± 16.00	
clorgyline						0.0070 ± 0.00070		
pargyline							140.0 ± 5.90	

[a]Results are the means ± standard errors from duplicate or triplicate experiments. [b]SI values are expressed for MAO-B compared with that for MAO-A. For tacrine (a reference compound for AChE and BChE), IC_{50} was confirmed by values of 270.0 ± 19.0 and 60.0 ± 2.2 nM, respectively. For donepezil (a reference compound for AChE and BChE), IC_{50} was confirmed by values of 9.5 ± 1.9 and 180.0 ± 3.8 nM, respectively. For quercetin (a reference compound for BACE1), IC_{50} was confirmed by the value of 13.4 ± 0.035 μM. For BACE inhibitor IV (a reference compound for BACE1), IC_{50} was confirmed by the value of 0.44 ± 0.064 μM.

selective MAO-B inhibitor (IC_{50} = 0.044 μM; K_i = 0.0080 ± 0.003 μM), with an SI value of 366.13.[18] We hypothesized that the electronic feature of the carbonyl group in a linker could be enhanced by two carbon−carbon double bond units. A recent study provided evidence that the presence of halogens on various MAO-B inhibitors significantly impacts the energetic stability of the inhibitor-binding cavities of these enzymes.[19]

Evidence from the recent design of MAO-B inhibitors showed the importance of halogens and extended conjugation in chalcone scaffolds. We obtained the framework of the title compound, which involved (1) extended conjugation of the three carbon linkers by adding an olefinic linkage to improve the electrophilic nature of the spacers, (2) addition of halogens at the para position of the chalcone ring A, and (3) introduction of electron-donating methoxyl and electron-withdrawing nitro groups at the para position of ring B of conjugated dienones (Figure 1).

On the other hand, AD is associated with a decrease in neurotransmitters, specifically acetylcholine (ACh), and with an increase in acetylcholinesterase (AChE) and/or butyrylcholinesterase (BChE).[20] In addition, β-secretase (β-site amyloid precursor protein-cleaving enzyme 1, BACE1) has been considered a target for AD treatment because it induces AD through the production of amyloid-β peptides.[21] Recently, multifunctional agents targeting MAO-A, MAO-B, AChE, BChE, and BACE1 have been studied for the effective treatment of AD.[22,23]

The current study synthesized a series of conjugated dienones (**MK1**−**MK15**) and investigated their in vitro MAO-A and MAO-B inhibitory profiles, including AChE, BChE, and BACE1 enzymes. The lead molecules were further subjected to kinetics, reversibility studies, assessment of cytotoxicity on normal cell lines, ROS assay, and molecular dynamics (MD) simulation.

RESULTS AND DISCUSSION

Chemistry. The multiconjugated dienones were synthesized by a pyrrolidine-catalyzed reaction between various substituted cinnamaldehyde derivatives and halogenated acetophenones (Scheme 1). All final derivatives were characterized using ^{1}H NMR, ^{13}C NMR, and mass spectrometry (see the Supporting Information).

Biochemistry. *MAO Inhibition Studies.* All compounds more effectively inhibited MAO-B than MAO-A and had strong inhibitory activities against MAO-B, with residual activities of <50% at 1 μM (Table 1). In general, (2*E*,4*E*)-1,5-diphenylpenta-2,4-dien-1-one derivatives (**MK1**−**MK15**) showed strong inhibitory activities against MAO-B. Compound **MK6** most potently inhibited MAO-B with an IC_{50} value of 2.82 nM, followed by **MK12** (IC_{50} = 3.22 nM) (Table 1). The −Br atom at the para position of **MK6** (a parent of the second subseries) increased the MAO-B inhibitory activity compared to the −Cl atom at the para position of **MK1** (IC_{50} = 11.17 nM—a parent of the first subseries). In the first subseries containing the −Cl atom at the para position, an NO_2 atom at the para position of **MK5** (IC_{50} = 4.02 nM) increased the MAO-B inhibitory activity compared to the parent **MK1**. In the second subseries containing the −Br atom at the para position, all derivatives substituted by other groups decreased the inhibitory activity against MAO-B. In the third subseries containing the −F atom at the para position, the methoxy group of **MK12** had the most effective inhibitory activity against MAO-B (IC_{50} = 3.22 nM), followed by the nitro group of **MK13** (IC_{50} = 4.24 nM). However, when the −F atom of **MK13** was replaced by the −H atom of **MK15**

https://doi.org/10.1021/acsomega.2c00397
ACS Omega 2022, 7, 8184−8197

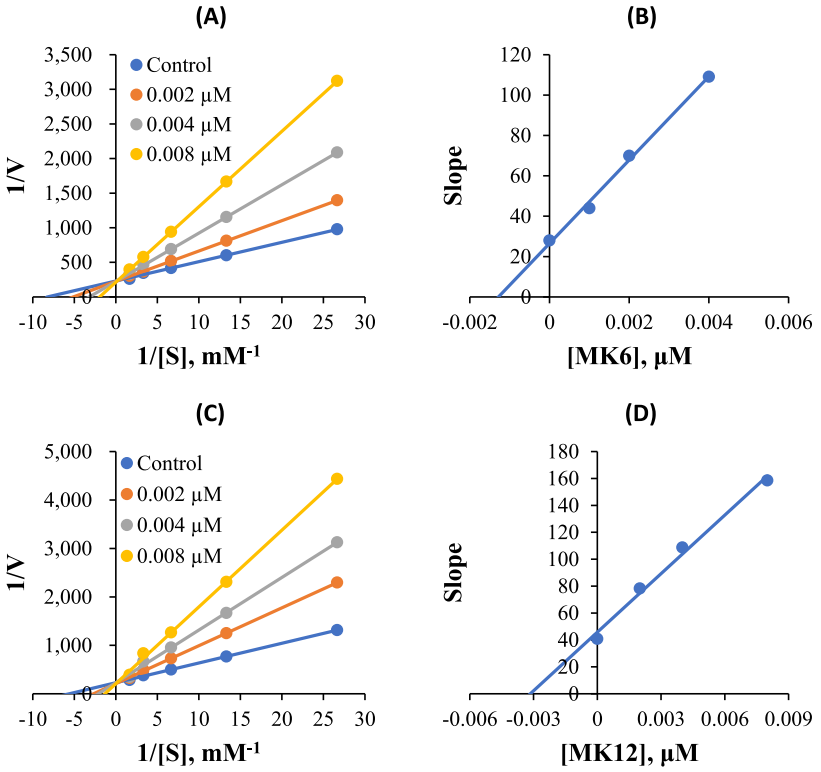

Figure 2. Lineweaver–Burk plots for MAO-B inhibition by **MK6** and **MK12** (A,C) and their respective secondary plots (B,D) of slopes vs inhibitor concentrations.

(IC_{50} = 12.4 nM), the inhibitory activity decreased. Moreover, the methoxy group and −F atom of **MK12** effectively inhibited both MAO-B and MAO-A (Table 1). **MK6** was selective for MAO-B, with an SI value of 7361.5 over MAO-A (Table 1). Multitarget analyses showed that all compounds weakly inhibited AChE, BChE, and β-secretase (BACE1) at 10 μM (Table 1).

Interestingly, all tested compounds showed significant MAO-B inhibitory activities compared to the reference drugs. The lead compounds **MK6** and **MK12** had potent MAO-B inhibitory activities (IC_{50} = 2.82 ± 0.39 and 3.22 ± 0.04 nM, respectively), which were 39 and 34 times more potent, respectively, than that of the reference reversible MAO-B drug lazabemide. These lead molecules also showed 50 and 44 times higher inhibitory activities, respectively, than the reference irreversible MAO-B inhibitor pargyline.

Kinetic Study. Based on kinetic studies of **MK6** and **MK12** for MAO-B, Lineweaver–Burk plots showed that the lines for **MK6** and **MK12** met at a point on the *y*-axis (Figure 2A,C), and their secondary plots had K_i values of 1.10 ± 0.20 and 3.00 ± 0.27 nM, respectively (Figure 3B,D). These results suggest that **MK6** and **MK12** are competitive inhibitors that bind at the active site of MAO-B.

Reversibility Studies. In the experiments, the concentration of **MK6** or **MK12** was 6.0 nM and that of lazabemide (a reference reversible inhibitor) and pargyline (a reference irreversible inhibitor) was 0.22 and 0.28 μM, respectively. The relative activities for undialyzed (A_U) and dialyzed (A_D) samples were compared to determine their reversibility patterns. The inhibition of MAO-B by **MK6** and **MK12** was recovered from 34.9% (A_U) to 79.2% (A_D) and from 33.4 to 74.7%, respectively (Figure 3). These recovery values were similar to those of lazabemide, a reversible reference inhibitor

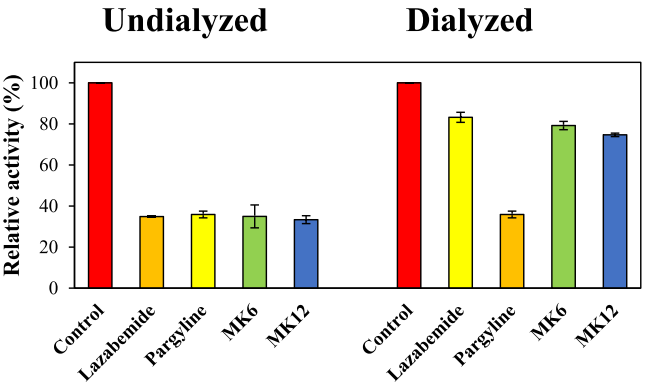

Figure 3. Recoveries of MAO-B inhibition by **MK6** and **MK12** using dialysis experiments.

against MAO-B (i.e., from 34.9 to 83.2%), and could be distinguished from pargyline, an irreversible reference inhibitor against MAO-B (i.e., from 35.9 to 35.9%). These results indicated that **MK6** and **MK12** were reversible inhibitors of MAO-B.

Cytotoxicity Studies of Vero Cells. We evaluated the biological safety of the effective compounds, such as **MK5**, **MK6**, **MK12**, and **MK14**, on a normal epithelial cell line from the kidney of an African green monkey (Vero cells) using the 3-(4,5-dimethylthiazol-2-yl)-2,5-diphenyltetrazolium bromide method. The Vero cells were treated with different concentrations (1–500 μg/mL) of the tested compounds for 24 h, and the relative cell viability was calculated at 570 nm using an ELISA microplate reader. The results showed that the compounds exhibited a percentage decrease in cell viability in a concentration-dependent manner (Figures 4a–7a). The IC_{50} values of **MK5**, **MK6**, **MK12**, and **MK14** were calculated as

https://doi.org/10.1021/acsomega.2c00397
ACS Omega 2022, 7, 8184–8197

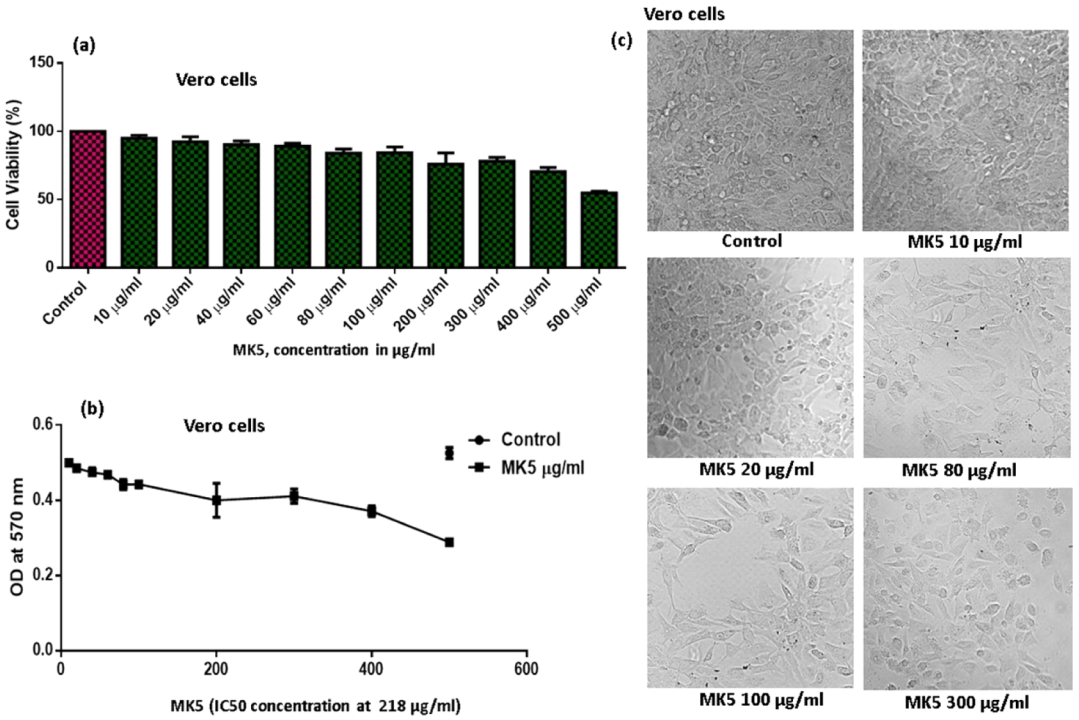

Figure 4. Effect of **MK5** on the cell viability of Vero cells: (a) cell viability >75% up to 300 μg/mL; (b) representation of a dose−response curve with an IC_{50} value of 218.4 μg/mL (696.1 μM); (c) morphological studies of Vero cells with different concentrations under a phase-contrast microscope, exposed for 24 h. The control value was 100%, and the data were presented as the means ± SEs from three independent experiments.

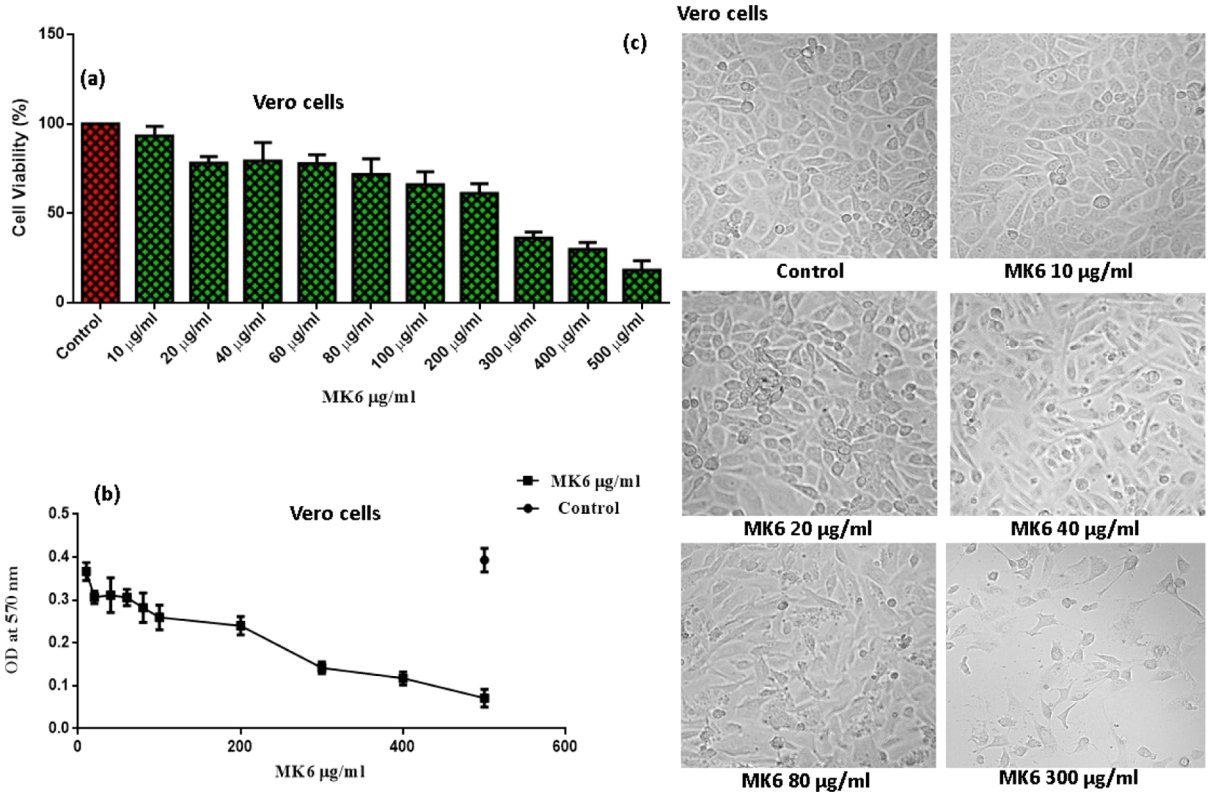

Figure 5. Effect of **MK6** on the cell viability of Vero cells: (a) cell viability > 70% at 80 μg/mL; (b) representation of a dose−response curve with an IC_{50} value of 149.1 μg/mL (476.1 μM); (c) morphological studies of Vero cells with different concentrations under a phase-contrast microscope, exposed for 24 h. The control value was taken as 100%, and the data were presented as the means ± SEs from three independent experiments.

218.4, 149.1, 99.96, and 162.3 μg/mL, respectively (Figures 4b−7b), from a dose−response curve plotted using the GraphPad Prism 6.0 software, whereas the EC_{50} values of the respective compounds were at the nanomolar level. The

https://doi.org/10.1021/acsomega.2c00397
ACS Omega 2022, 7, 8184−8197

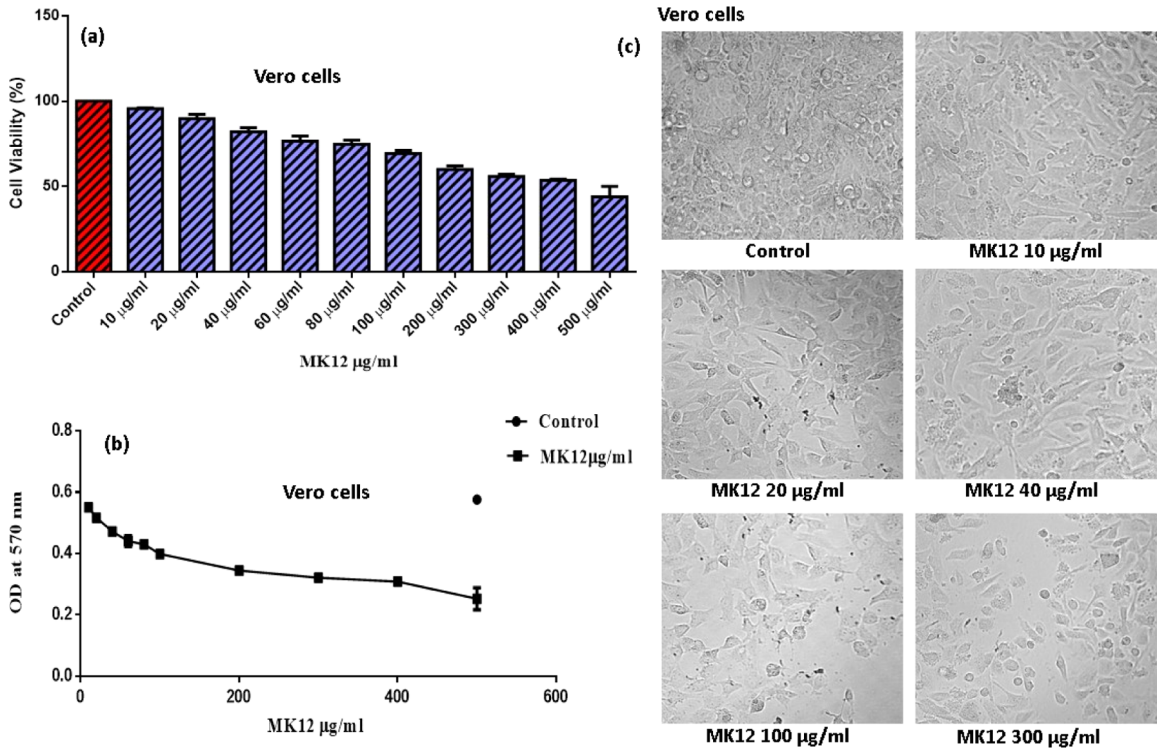

Figure 6. Effect of **MK12** on the cell viability of Vero cells: (a) cell viability >80% at 40 μg/mL; (b) representation of a dose−response curve with an IC_{50} value of 99.96 μg/mL (354.1 μM); (c) morphological studies of Vero cells with different concentrations under a phase-contrast microscope, exposed for 24 h. The control value was 100%, and the data were presented as the means ± SEs from three independent experiments.

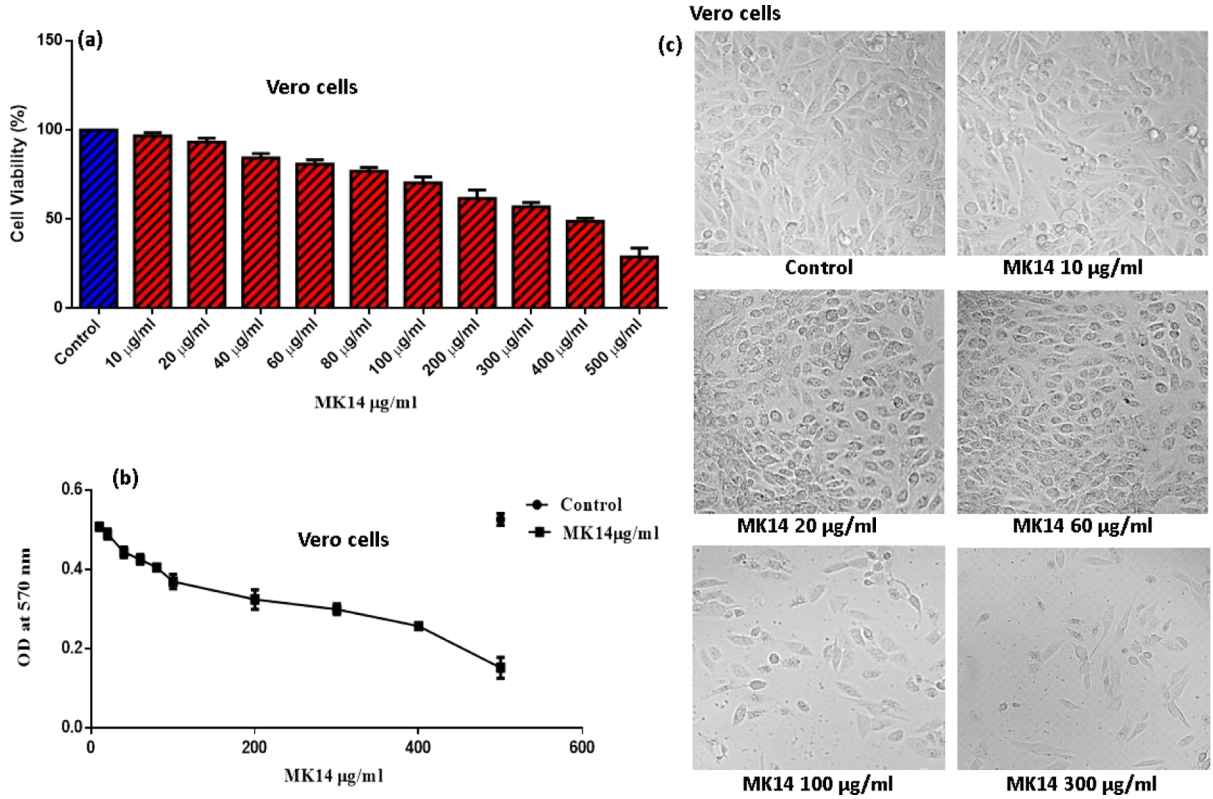

Figure 7. Effect of **MK14** on the cell viability of Vero cells: (a) cell viability >80% at 60 μg/mL; (b) representation of a dose−response curve with an IC_{50} value of 162.3 μg/mL (614.0 μM); (c) morphological studies of Vero cells with different concentrations under a phase-contrast microscope, exposed for 24 h. The control value was 100%, and the data were presented as the means ± SEs from three independent experiments.

https://doi.org/10.1021/acsomega.2c00397
ACS Omega 2022, 7, 8184−8197

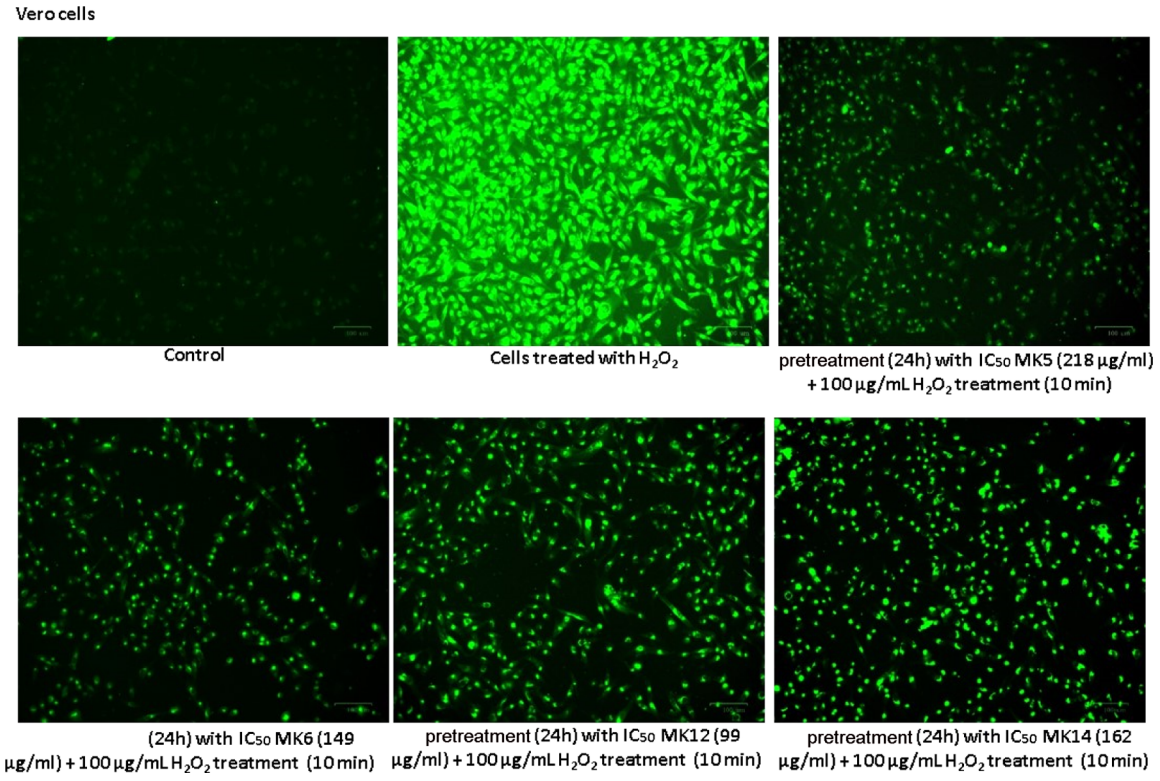

Figure 8. Effects of **MK5**, **MK6**, **MK12**, and **MK14** on ROS levels induced by H_2O_2. Vero cells were pretreated with respective drugs for 24 h. These cells were exposed to 100 μg/mL H_2O_2 for 10 min, and ROS production was evaluated.

Table 2. MM/PBSA Binding Free Energy Profiles of MK5, MK6, MK12, and MK14

compounds	ΔE_{vdw} (kcal/mol)	ΔE_{ele} (kcal/mol)	ΔG_{gas} (kcal/mol)	ΔG_{sol} (kcal/mol)	ΔG_{bind} (kcal/mol)
MK5	−45.41 ± 0.04	−7.97 ± 0.04	−53.38 ± 0.05	12.52 ± 0.03	−40.86 ± 0.04
MK6	−46.77 ± 0.05	−10.70 ± 0.06	−57.47 ± 0.07	14.00 ± 0.04	−43.47 ± 0.07
MK12	−50.44 ± 0.04	−4.59 ± 0.04	−55.03 ± 0.05	13.35 ± 0.03	−41.69 ± 0.05
MK14	−43.16 ± 0.04	−9.76 ± 0.05	−52.92 ± 0.05	13.99 ± 0.03	−38.92 ± 0.04

biological safety of the compounds was found to be in the order of **MK5** > **MK14** > **MK6** > **MK12**. Additionally, the effect of the compounds on cellular morphology was analyzed using phase-contrast microscopy. The cell membrane integrity and reduction in cell numbers associated with cellular viability were demonstrated morphologically in the Vero cells. The results indicated that **MK5**, **MK6**, and **MK14** exhibited no signs of toxicity at a concentration of 100 μg/mL (Figures 4c, 5c, and 7c), whereas **MK12** (Figure 6c) was the most toxic of the four tested compounds. The cells exposed to higher concentrations (300 μg/mL) showed the marked morphological alterations typically associated with cytotoxicity, such as a marked reduction in cellular density, cellular shrinkage, and blebbing. This study revealed that **MK5**, **MK6**, **MK12**, and **MK14** were biologically safe compounds with IC_{50} values ≥100 μg/mL, and the effective concentration of the compounds was at a level of <10 nM.

ROS Assay. The effect of **MK5**, **MK6**, **MK12**, and **MK14** on intracellular ROS scavenging was tested using Vero cells. The cells were exposed to H_2O_2 for excess ROS generation for 10 min, and the respective drugs were treated as described previously.[24] The images were taken under a fluorescence microscope. Following drug treatment, the intracellular ROS generation in H_2O_2-treated Vero cells decreased, and calculation of the intensity of fluorescence after 24 h of drug treatment indicated balanced pro-oxidant and antioxidant levels in the cell system (Figure 8a−d). The effective compounds **MK5**, **MK6**, **MK12**, and **MK14** exhibited a significant ROS scavenging effect compared with H_2O_2-treated control cells. Excess generation of ROS has been reported to induce oxidative stress in the brain, thereby leading to neuronal damage in neurodegenerative diseases. Severe nerve damage can be controlled by balancing ROS generation and scavenging by antioxidants.[25] This study concluded that the effective compounds efficiently controlled the ROS produced by H_2O_2 treatment, and they were biologically safe. The compounds may be considered future therapeutics if their efficacy is further confirmed by preclinical trials.

Computational Studies. *Computational Analysis Based on the MM/PBSA Method.* The binding modes of the lead molecules **MK5**, **MK6**, **MK12**, and **MK14** were established using the MM/PBSA method. Binding free energy provides insights into the binding affinity of a compound with its target, and it is an important parameter for hit-to-lead and lead optimization in drug discovery.[26] Binding affinity estimations of the compounds would therefore provide insights into the molecular basis of their activity against MAO-B. In this report, we employed the MM/PBSA approach, which has been widely used to estimate binding free energies due to its reliability and cheaper cost than experimental methods.[27] To calculate

https://doi.org/10.1021/acsomega.2c00397
ACS Omega 2022, 7, 8184−8197

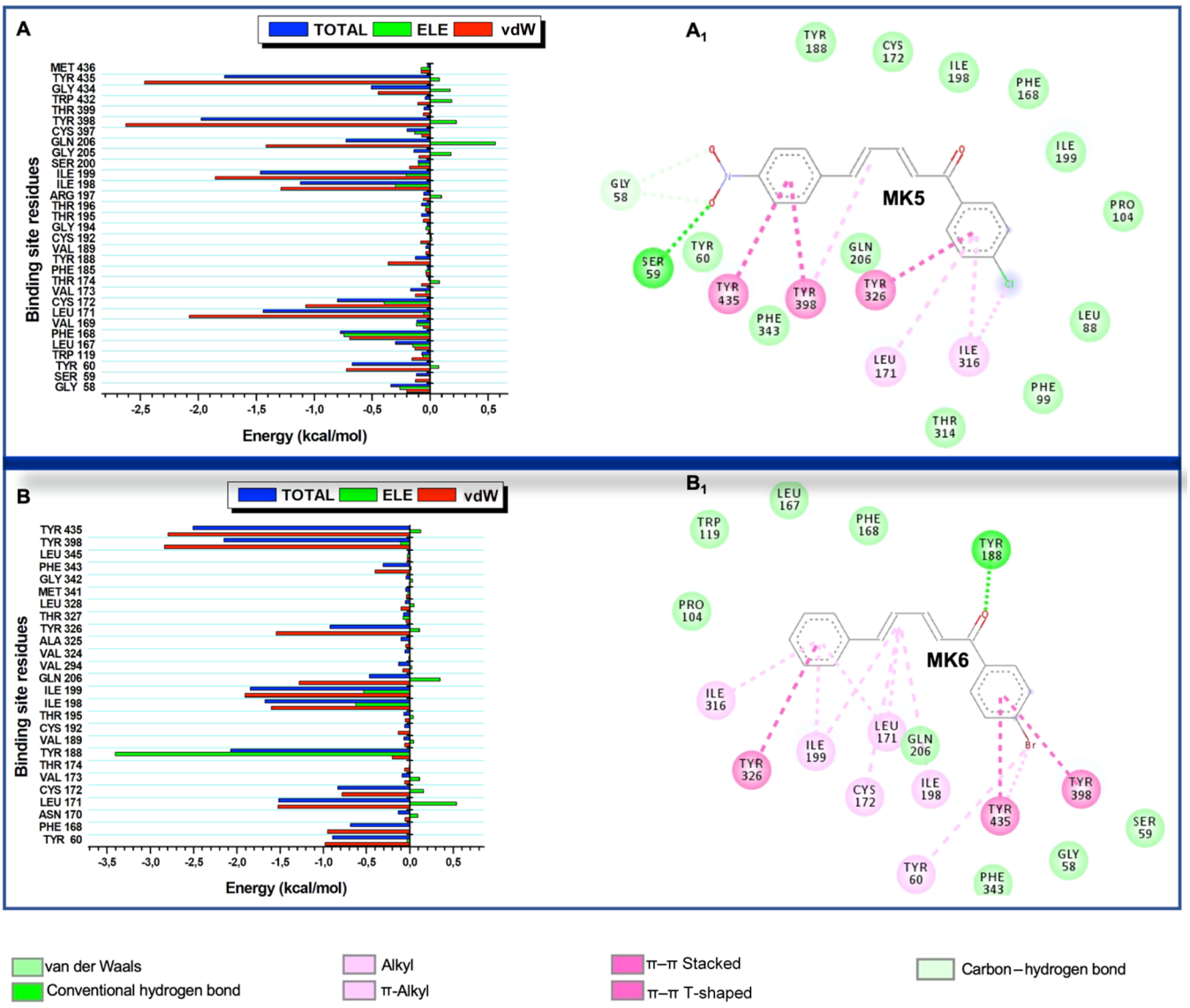

Figure 9. Per-residue energy contribution plot and corresponding ligand interaction profile of MAO-B binding pocket residues in a complex of **MK5** (A) and **MK6** (B). The ligand interaction profile highlighted the accompanying interactions and revealed the contributed binding free energies.

binding free energy, snapshots taken between 100 and 200 ns were used to ensure that all the simulated models had equilibrated. The MM/PBSA method considers several energy contributions, including van der Waals (vdW) and electrostatic interactions, polar solvation energy, and nonpolar solvent-accessible surface area energy. Entropy energy contributions were not considered because this research investigated each compound's binding only to MAO-B but with different binding modes; hence, entropic energy contributions would have produced minimal differences between binding modes. The degree of binding affinity reflected the strength of interactions between the compounds and MAO-B and therefore indicated their inhibitory potential. The MM/PBSA calculation results, presented in Table 2, showed estimated total binding free energies of −40.86, −43.47, −41.69, and −38.92 kcal/mol for **MK5**, **MK6**, **MK12**, and **MK14**, respectively. Of the compounds, **MK14** exhibited the highest binding free energy, while **MK12** (−38.92 kcal/mol) had the lowest binding free energy. Overall, all the compounds had favorable binding affinities with MAO-B, characterized by the high energy contributions of vdW and electrostatic interactions with binding site residues, which supported our experimental findings, with IC_{50} values for **MK5**, **MK6**, **MK12**, and **MK14** of 0.0040, 0.0028, 0.0032, and 0.0049 μM, respectively. These values corresponded with high binding affinities and reflected the favorable functional strength of each compound as a potential drug.

Binding Site Energetics That Characterize MK5, MK6, MK12, and MK14 Binding. Having estimated the binding free energies of **MK5**, **MK6**, **MK12**, and **MK14** toward MAO-B, we proceeded to explore the energetics of each binding site by quantifying the energy contribution of each binding site residue using the per-residue energy decomposition component of the MM/PBSA approach in AMBER 18.[28] Decomposition of the energetics of the binding site residues allowed us to identify residues that were crucial to the binding of each residue while providing a molecular perspective on the possible binding mechanism of each compound. Residues that contributed total energies ≤−1 kcal/mol were considered crucial to the binding of the corresponding compound and

https://doi.org/10.1021/acsomega.2c00397
ACS Omega 2022, 7, 8184−8197

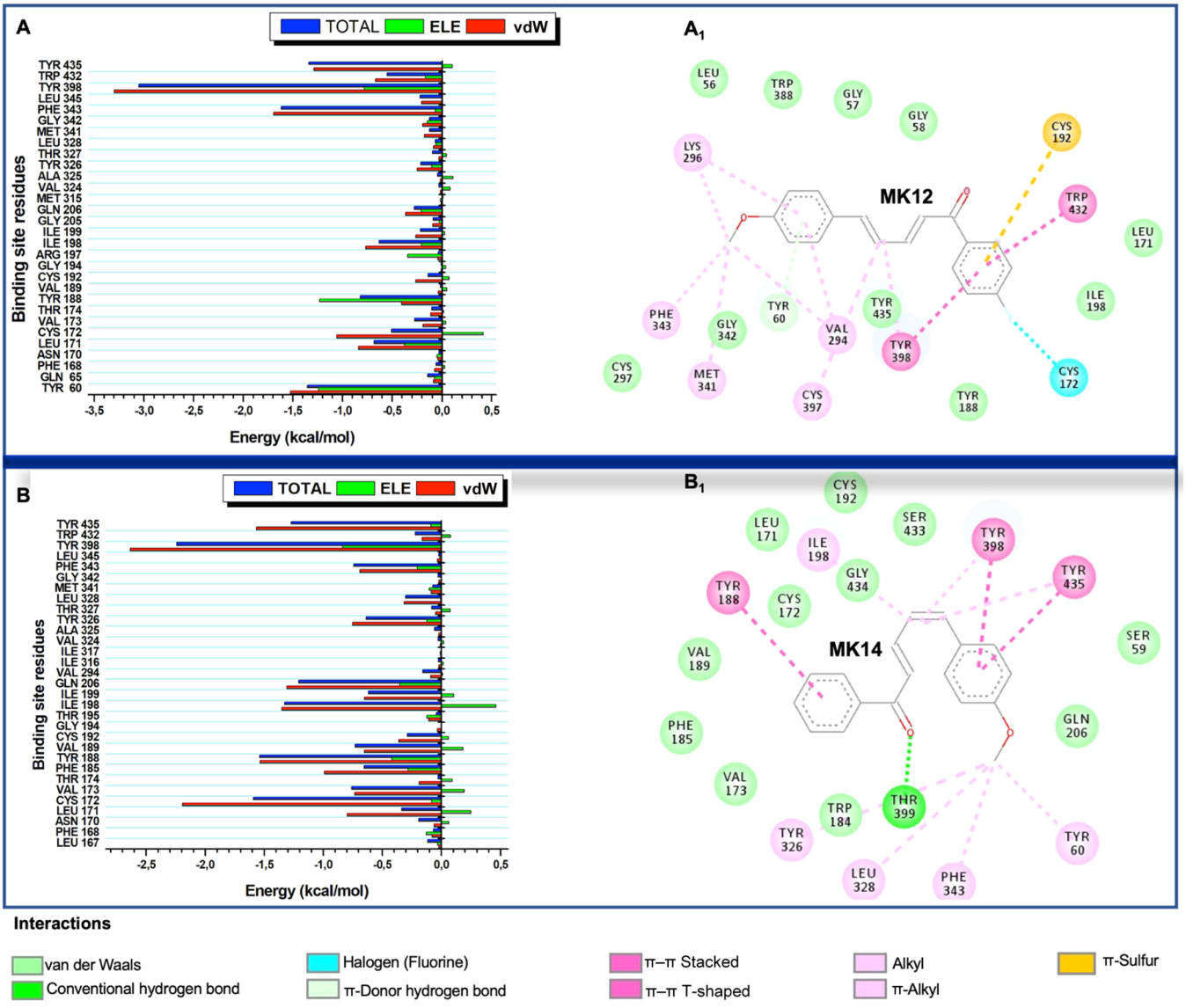

Figure 10. Per-residue energy contribution plot and corresponding ligand interaction profile of MAO-B binding pocket residues in a complex of **MK12** (A) and **MK14** (B). The ligand interaction profile highlighted the accompanying interactions and revealed the contributed binding free energies.

could inform future drug design processes for novel MAO-B inhibitors. As shown in Figure 9A, the major interactions constituting the binding of **MK5** included LEU171 (−1.44 kcal/mol), ILE198 (−1.12 kcal/mol), ILE199 (−1.47 kcal/mol), TYR398 (−1.97 kcal/mol), and TYR435 (−1.78 kcal/mol). These residues were shown to correspondingly engage in high-affinity interactions with **MK5**, as shown in Figure 9A_1. The major residues involved in the binding mechanism of **MK6** included LEU171 (−1.51 kcal/mol), TYR188 (−2.07 kcal/mol), ILE199 (−1.85 kcal/mol), TYR398 (−2.15 kcal/mol), and TYR435 (−2.51 kcal/mol), as evidenced by high-affinity interactions, such as conventional hydrogen bonds, $\pi-\pi$ stacked−T-shaped interactions, and π-alkyl−alkyl interactions, as shown in Figure 9B,B_1. These high-affinity interactions culminated in the highest binding free energy of **MK6** compared to the other compounds.

Based on the per-residue energy decomposition of the **MK12**−MAO-B complex, the major binding site residues that were identified as crucial in the binding process included TYR60 (−1.35 kcal/mol), PHE343 (−1.62 kcal/mol), TYR398 (−3.05 kcal/mol), and TYR435 (−1.34 kcal/mol), as shown in Figure 10A. The **MK12** binding was also characterized by notable interactions, such as $\pi-\pi$ stacked−T-shaped interactions, π−sulfur interaction, and halogen interaction, as shown in Figure 10A_1. Likewise, the crucial residues that contributed to the binding of **MK14** included CYS172 (−1.59 kcal/mol), TYR188 (−1.53 kcal/mol), ILE198 (−1.33 kcal/mol), GLN206 (−1.21 kcal/mol), TYR398 (−2.24 kcal/mol), and TYR435 (−1.27 kcal/mol), as shown in Figure 10B. These residues mediated high-affinity interactions, such as $\pi-\pi$ stacked−T-shaped interactions, π-alkyl−alkyl interactions, and conventional hydrogen bonds, as shown in Figure 10B_1. Overall, **MK5**, **MK6**, **MK12**, and **MK14** bind favorably to MAO-B, as shown by high-affinity interactions with specific residues, and a pool of vdW interactions, which stabilized each compound within the MAO-B binding pocket to facilitate the inhibitory activity.

https://doi.org/10.1021/acsomega.2c00397
ACS Omega 2022, 7, 8184−8197

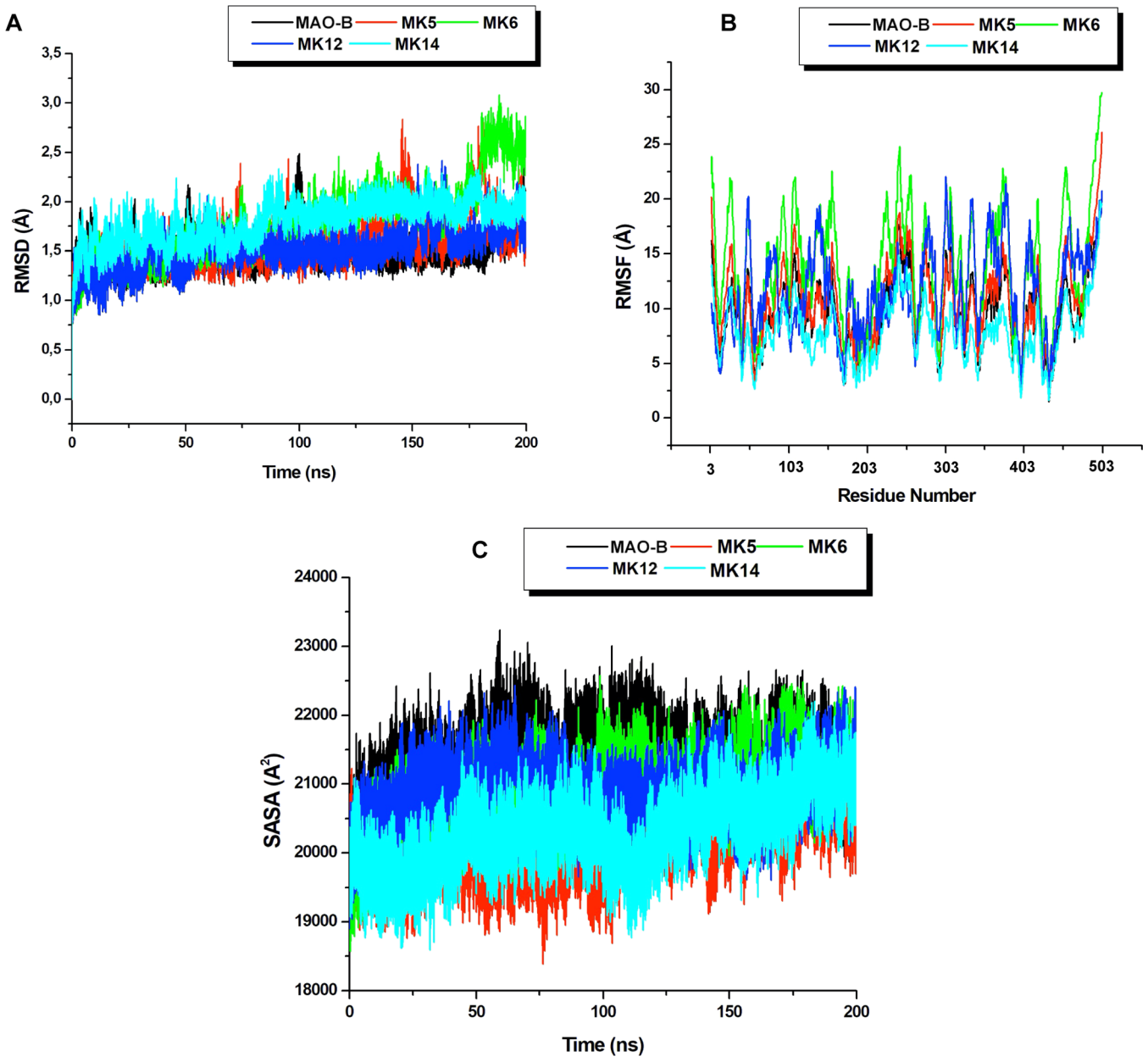

Figure 11. Structural and conformational analysis. (A) Comparative RMSD plots of the inhibitor-bound MAO-B and the unbound MAO-B; (B) comparative RMSF plots showing per-residue fluctuations across the 200 ns simulation period for the inhibitor-bound MAO-B and the unbound MAO-B; (C) comparative SASA plots for the inhibitor-bound MAO-B and the unbound MAO-B across the 200 ns MD simulation period.

Table 3. Average RMSD, RMSF, and SASA Estimations for Simulated Models over 200 ns

parameter	APO	MK5	MK6	MK12	MK14
RMSD (Å)	1.56	1.71	1.89	1.56	1.84
RMSF (Å)	9.69	10.71	14.06	11.62	7.80
SASA (Å^2)	21,423.24	20,308.47	20,970.32	20,973.83	20,457.29

*Structural and Conformational Implications of the Binding of **MK5**, **MK6**, **MK12**, and **MK14**.* The therapeutic binding of chemical compounds with biological targets is usually associated with various conformational and structural changes that interfere with the normal functions of the biological targets.[29] The MD simulation performed in this research allowed for a nanosecond assessment of the structural changes associated with the MAO-B binding of each compound. The crucial parameters assessed to provide insights into the structural changes included enzyme structure stability, enzyme structure flexibility, and enzyme folding/unfolding dynamics.[30,31] These were computed by estimating the C-α root-mean-square deviation (RMSD),[32] C-α root-mean-square fluctuation (RMSF),[33] and solvent accessible surface area (SASA)[34] of the trajectories generated after the 200 ns MD simulation.

The C-α RMSD measures atomistic deviations and reflects the stability and convergence of simulated models. As observed

https://doi.org/10.1021/acsomega.2c00397
ACS Omega 2022, 7, 8184−8197

in Figure 11, all the simulated models converged after about 100 ns, leading to ensuing deviations being attributed to the presence or absence of a bound ligand. The initial increase in deviations from the start of the simulation up to about 100 ns resulted from initial atomic expansions. As shown in the table and Figure 11A, although the binding of **MK5**, **MK6**, **MK12**, and **MK14** generally increased the RMSD of the C-α atoms of MAO-B, as evidenced by the relatively higher average RMSD of the inhibitor-bound systems, the structure of MAO-B remained generally stable over the simulation period, with an average RMSD below 2 Å. As shown in Table 3, **MK5**, **MK6**, **MK12**, and **MK14** exhibited average RMSDs of 1.71, 1.89, 1.56, and 1.84 Å, respectively, and the unbound MAO-B also had an average RMSD of 1.56 Å. This suggested that the binding of the compounds with MAO-B was characterized by an increase in the stability of MAO-B—a feature that could favor binding interaction dynamics.[35] The RMSF (a parameter that predicted the residue flexibility of individual residues of MAO-B in the presence or absence of compounds) was also calculated. As observed from the RMSF plots in Figure 11 and Table 3, individual residues in the unbound MAO-B exhibited relatively lower average RMSFs, suggesting lower residue flexibility. Comparatively, individual residues in the inhibitor-bound MAO-B, except for the **MK14**-bound system, exhibited relatively higher average RMSFs than the unbound MAO-B, suggesting that the binding of **MK5**, **MK6**, and **MK12** induced residue flexibility, which could interfere with the function of MAO-B, leading to the observed inhibitory activity and high binding affinity. **MK14**, on the other hand, decreased the flexibility of individual residues, as evidenced by an average RMSF of 7.80 Å. The decreased residue flexibility could have impeded crucial binding interactions resulting in the low binding affinity calculated for **MK14**.

Furthermore, using SASA calculations, we investigated the impact of inhibitor binding on the folding and unfolding of MAO-B, considering the importance of this phenomenon for enzyme functioning.[36] Unfolding/folding of the enzyme structure could impede or expose individual residues to solvent surfaces, thereby interfering with binding interactions and enzyme functioning. As observed in Figure 11 and Table 3, the unbound MAO-B had a relatively higher average SASA of 21423.24 Å^2 compared with all the bound conformations of MAO-B. This suggested that, following binding of **MK5**, **MK6**, **MK12**, and **MK14**, the individual residues of MAO-B underwent structural rearrangement consistent with structural folding, the burial of hydrophobic residues, and a reduction in exposure to solvent surfaces, which tended to influence the functioning of MAO-B. Of the compounds, the **MK5**-bound complex had the highest folding, with an average SASA of 20308.47 Å^2, whereas the least folding occurred in the **MK12** complex, with an average SASA of 20973.83 Å^2. Overall, the similarity in the binding dynamics of the compounds suggested similarity in the structural mechanisms of inhibition characterized by distortion of the conformational dynamics of MAO-B.

CONCLUSIONS

In this study, 15 halogen-bearing multiconjugated dienones were synthesized and evaluated for their human MAOs, ChEs, and BACE1 inhibition. Surprisingly, all derivatives showed a potent selective MAO-B inhibitory activity in the nanomolar range compared to the reference drugs. **MK6** had the most potent inhibitory activity against MAO-B, with an IC_{50} value of 2.82 nM, followed by **MK12** (IC_{50} = 3.22 nM). Kinetic and reversibility studies showed that **MK6** and **MK12** were competitive and reversible inhibitors of MAO-B. These compounds exhibited no distinct signs of toxicity on normal Vero cells in in vitro toxicity studies. Additionally, pro-oxidant and antioxidant levels were retained by **MK6** and **MK12**. The MD studies provided novel insights into the binding modes of the inhibitor-binding cavity of MAO-B. Therefore, this study suggests that **MK6** and **MK12** have therapeutic potential for the treatment of various neurodegenerative disorders, such as AD and PD.

MATERIALS AND METHODS

Synthesis. Acetophenone/halogenated acetophenones (0.01 M) were added to a stirred solution of the respective cinnamaldehyde derivatives (0.01 M) in 20 mL of ethanol using a micropipette. Pyrrolidine (0.01 M) was added to the mixture immediately, which soon changed to a brown or orange color. Overnight stirring resulted in multiconjugated ketones after the addition of ice cubes, which were filtered under suction, washed thoroughly with water, and then dried in a desiccator overnight.[37]

*(2E,4E)-1-(4-Chlorophenyl)-5-phenylpenta-2,4-dien-1-one (**MK1**).* mp 118−120 °C; ^{1}H NMR (500 MHz, chloroform-*d*): δ 7.98−7.91 (m, 2H), 7.63 (dd, *J* = 14.9, 7.7, 2.7 Hz, 1H), 7.55−7.47 (m, 4H), 7.43−7.33 (m, 3H), 7.10−7.03 (m, 3H); ^{13}C NMR (125 MHz, $CDCl_3$): δ 189.2, 145.4, 142.5, 139.2, 139.1, 136.7, 136.0, 129.8, 129.3, 128.9, 127.4, 126.8, 124.8. Molecular formula $C_{17}H_{13}ClO$ (HRMS): calculated = 268.7375, observed = 268.7398.

*(2E,4E)-5-(4-Bromophenyl)-1-(4-chlorophenyl)penta-2,4-dien-1-one (**MK2**).* mp 138−140 °C; ^{1}H NMR (500 MHz, chloroform-*d*): δ 7.96−7.88 (m, 2H), 7.58 (dd, *J* = 14.9, 10.0 Hz, 1H), 7.52−7.41 (m, 4H), 7.39−7.33 (m, 2H), 7.06 (d, *J* = 14.9 Hz, 1H), 7.03−6.92 (m, 2H); ^{13}C NMR (125 MHz, $CDCl_3$): δ 189.0, 144.8, 140.8, 139.2, 134.9, 132.1, 129.8, 128.9, 128.7, 127.4, 125.3, 123.3. Molecular formula $C_{17}H_{12}ClBr$ (HRMS): calculated = 347.6335, observed = 347.6298.

*(2E,4E)-1-(4-Chlorophenyl)-5-(4-methoxyphenyl)penta-2,4-dien-1-one (**MK3**).* mp 119−121 °C; ^{1}H NMR (500 MHz, chloroform-*d*): δ 7.95−7.87 (m, 2H), 7.61 (dd, *J* = 14.7, 10.9 Hz, 1H), 7.49−7.42 (m, 4H), 7.00 (d, *J* = 15.1 Hz, 2H), 6.96−6.85 (m, 3H), 3.84 (s, 3H); ^{13}C NMR (125 MHz, $CDCl_3$): δ 189.2, 160.7, 145.9, 142.3, 138.9, 136.7, 129.7, 128.9, 128.8, 124.7, 123.6, 114.3, 55.4. Molecular formula $C_{18}H_{15}ClO_2$ (HRMS): calculated = 298.7635, observed = 298.7698.

*(2E,4E)-1-(4-Chlorophenyl)-5-(4-fluorophenyl)penta-2,4-dien-1-one (**MK4**).* mp 134−136 °C; ^{1}H NMR (500 MHz, chloroform-*d*): δ 7.99−7.88 (m, 2H), 7.59 (dd, *J* = 14.9, 10.4 Hz, 1H), 7.47 (tt, *J* = 8.9, 2.3 Hz, 4H), 7.08−7.05 (m, 2H), 7.02 (d, *J* = 6.4 Hz, 1H), 6.99−6.89 (m, 2H); ^{13}C NMR (125 MHz, $CDCl_3$): δ 189.1, 162.3, 145.1, 141.0, 139.1, 129.8, 129.1, 129.0, 128.9, 126.5, 124.8, 116.1. Molecular formula $C_{17}H_{12}ClFO$ (HRMS): calculated = 286.7279, observed = 286.7298.

*(2E,4E)-1-(4-Chlorophenyl)-5-(4-nitrophenyl)penta-2,4-dien-1-one (**MK5**).* mp 120−121 °C; ^{1}H NMR (500 MHz, chloroform-*d*): δ 8.25−8.22 (m, 2H), 7.94−7.90 (m, 1H), 7.65−7.56 (m, 3H), 7.50−7.45 (m, 2H), 7.22−7.02 (m, 12H); ^{13}C NMR (125 MHz, $CDCl_3$): δ 188.7, 147.7, 143.6, 142.2, 139.5, 138.9, 136.1, 130.8, 129.8, 129.0, 127.6, 127.2, 124.2.

https://doi.org/10.1021/acsomega.2c00397
ACS Omega 2022, 7, 8184−8197

Molecular formula $C_{17}H_{12}ClNO_3$ (HRMS): calculated = 313.7345, observed = 313.7398.

*(2E,4E)-1-(4-Bromophenyl)-5-phenylpenta-2,4-dien-1-one (**MK6**).* mp 132−134 °C; ^{1}H NMR (500 MHz, chloroform-*d*): δ 7.85−7.83 (m, 2H), 7.64−7.62 (m, 3H), 7.53−7.48 (m, 2H), 7.40−7.32 (m, 3H), 7.07−7.00 (m, 3H); ^{13}C NMR (125 MHz, $CDCl_3$): δ 189.3, 145.4, 142.4, 136.9, 136.0, 131.9, 129.9, 129.3, 128.9, 127.3, 126.7, 124.8. Molecular formula $C_{17}H_{13}BrO$ (HRMS): calculated = 313.1885, observed = 313.1898.

*(2E,4E)-1,5-Bis(4-bromophenyl)penta-2,4-dien-1-one (**MK7**).* mp 128−130 °C; ^{1}H NMR (500 MHz, chloroform-*d*): δ 7.85−7.83 (m, 2H), 7.66−7.62 (m, 2H), 7.58 (dd, *J* = 14.9, 9.9 Hz, 1H), 7.54−7.46 (m, 2H), 7.39−7.33 (m, 2H), 7.08−6.96 (m, 3H); ^{13}C NMR (125 MHz, $CDCl_3$): δ 189.2, 144.8, 140.8, 136.8, 134.9, 132.1, 131.9, 129.9, 128.7, 127.4, 125.2, 123.4. Molecular formula $C_{17}H_{12}Br_2O$ (HRMS): calculated = 392.0845, observed = 392.0899.

*(2E,4E)-1-(4-Bromophenyl)-5-(4-methoxyphenyl)penta-2,4-dien-1-one (**MK8**).* MP, 138−140 °C; ^{1}H NMR (500 MHz, chloroform-*d*): δ 7.87−7.79 (m, 2H), 7.65−7.56 (m, 3H), 7.48−7.42 (m, 2H), 7.03−6.95 (m, 2H), 6.94−6.85 (m, 3H), 3.84 (s, 3H); ^{13}C NMR (125 MHz, $CDCl_3$): δ 189.3, 160.7, 146.0, 142.3, 137.1, 131.8, 129.8, 128.9, 128.8, 127.5, 124.7, 123.6, 114.4, 55.4. Molecular formula $C_{18}H_{15}BrO_2$ (HRMS): calculated = 343.2145, observed = 343.2196.

*(2E,4E)-1-(4-Bromophenyl)-5-(4-fluorophenyl)penta-2,4-dien-1-one (**MK9**).* mp 160−162 °C; ^{1}H NMR (500 MHz, chloroform-*d*): δ 7.88−7.80 (m, 2H), 7.68−7.54 (m, 3H), 7.52−7.44 (m, 2H), 7.12−6.89 (m, 5H); ^{13}C NMR (125 MHz, $CDCl_3$): δ 189.3, 145.2, 141.0, 136.9, 131.9, 129.9, 129.1, 129.0, 127.8, 126.5, 124.8, 116.1, 115.9. Molecular formula $C_{17}H_{12}BrFO$ (HRMS): calculated = 331.1789, observed = 331.1798.

*(2E,4E)-1-(4-Bromophenyl)-5-(4-nitrophenyl)penta-2,4-dien-1-one (**MK10**).* mp 148−150 °C; ^{1}H NMR (500 MHz, chloroform-*d*): δ 8.27−8.22 (m, 2H), 7.90−7.76 (m, 2H), 7.68−7.57 (m, 5H), 7.19−7.10 (m, 2H), 7.06 (d, *J* = 15.6 Hz, 1H); ^{13}C NMR (125 MHz, $CDCl_3$): δ 188.9, 147.7, 143.6, 142.2, 136.5, 132.0, 130.8, 129.9, 128.2, 127.7, 127.1, 124.2. Molecular formula $C_{17}H_{12}BrNO_3$ (HRMS): calculated = 358.1855, observed = 360.2098.

*(2E,4E)-5-(4-Bromophenyl)-1-(4-fluorophenyl)penta-2,4-dien-1-one (**MK11**).* mp 121−123 °C; ^{1}H NMR (500 MHz, chloroform-*d*): δ 8.00 (dd, *J* = 7.9, 5.0, 2.3 Hz, 2H), 7.76−7.67 (m, 1H), 7.53−7.44 (m, 3H), 7.38−7.35 (m, 2H), 7.19−7.09 (m, 4H); ^{13}C NMR (125 MHz, $CDCl_3$): δ 188.7, 144.5, 140.6, 134.9, 132.2, 132.0, 131.9, 131.0, 130.9, 129.7, 129.3, 128.6, 127.4. Molecular formula $C_{17}H_{12}BrFO$ (HRMS): calculated = 331.1789, observed = 331.1798.

*(2E,4E)-1-(4-Fluorophenyl)-5-(4-methoxyphenyl)penta-2,4-dien-1-one (**MK12**).* mp 100−102 °C; ^{1}H NMR (500 MHz, chloroform-*d*): δ 8.05−7.96 (m, 2H), 7.60 (dd, *J* = 14.9, 10.8 Hz, 1H), 7.48−7.42 (m, 2H), 7.22−7.11 (m, 2H), 7.05−6.95 (m, 2H), 6.95−6.83 (m, 3H), 3.84 (s, 3H); ^{13}C NMR (125 MHz, $CDCl_3$): δ 188.8, 160.7, 145.6, 142.1, 130.9, 130.8, 128.9, 124.7, 123.7, 115.7, 115.5, 114.3, 55.3. Molecular formula $C_{18}H_{15}FO_2$ (HRMS): calculated = 282.3089, observed = 282.3097.

*(2E,4E)-1-(4-Fluorophenyl)-5-(4-nitrophenyl)penta-2,4-dien-1-one (**MK13**).* mp 117−119 °C; ^{1}H NMR (500 MHz, chloroform-*d*): δ 8.26−8.21 (m, 2H), 8.06−7.98 (m, 2H), 7.67−7.54 (m, 3H), 7.21−7.11 (m, 4H), 7.06 (d, *J* = 15.5 Hz, 1H); ^{13}C NMR (125 MHz, $CDCl_3$): δ 188.4, 147.7, 143.3, 138.7, 131.1, 131.0, 130.9, 127.7, 127.3, 124.2, 115.9, 115.7. Molecular formula $C_{17}H_{12}FNO_3$ (HRMS): calculated = 297.2799, observed = 297.2899.

*(2E,4E)-5-(4-Methoxyphenyl)-1-phenylpenta-2,4-dien-1-one (**MK14**).* mp 76−78 °C; ^{1}H NMR (500 MHz, chloroform-*d*): δ 8.00−7.94 (m, 2H), 7.65−7.52 (m, 2H), 7.53−7.41 (m, 4H), 7.10−6.85 (m, 20H), 3.84 (s, 3H); ^{13}C NMR (125 MHz, $CDCl_3$): δ 190.6, 160.6, 145.4, 141.8, 138.4, 132.5, 128.9, 128.8, 128.5, 128.3, 124.9, 124.3, 114.3, 55.3. Molecular formula $C_{18}H_{16}O_2$ (HRMS): calculated = 264.3184, observed = 264.3198.

*(2E,4E)-5-(4-Nitrophenyl)-1-phenylpenta-2,4-dien-1-one (**MK15**).* mp 118−120 °C; ^{1}H NMR (500 MHz, chloroform-*d*): δ 8.26−8.22 (m, 2H), 8.00−7.97 (m, 2H), 7.75−7.56 (m, 4H), 7.51 (dd, *J* = 8.4, 7.0 Hz, 2H), 7.25−7.13 (m, 2H), 7.05 (d, *J* = 15.6 Hz, 1H); ^{13}C NMR (125 MHz, $CDCl_3$): δ 190.1, 143.1, 142.3, 138.5, 137.8, 133.0, 131.1, 128.7, 128.4, 127.8, 127.6, 124.2, 77.2. Molecular formula $C_{17}H_{13}NO_3$ (HRMS): calculated = 279.2894, observed = 279.2998.

Enzyme Assays. MAO inhibitory activities were assayed by recombinant MAO-A and MAO-B using kynuramine (0.06 mM) and benzylamine (0.3 mM) as substrates.[38] Toloxatone and clorgyline were used as reference compounds for MAO-A, and lazabemide and pargyline were used for MAO-B. The K_m of benzylamine for MAO-B was 0.17−0.18 mM.[39] For multitarget analysis, AChE, BChE, and BACE1 inhibitory activities were tested as described previously.[40]

Enzyme Inhibition and Kinetic Studies. The inhibitory activities of **MK1**−**MK15** against MAOs were first screened at 10 μM. For the compounds showing <50% residual activities, we determined the IC_{50} values of the compounds. The SI values of MAO-B were expressed by calculating IC_{50} (MAO-A)/IC_{50} (MAO-B). Enzyme kinetics were determined for compounds **MK6** and **MK12** with MAO-B at five different substrate concentrations. The inhibition patterns were analyzed using Lineweaver−Burk plots and their secondary plots for three inhibitor concentrations.[41−43]

Inhibition Reversibility of MK6 and MK12. The dialysis method was used for the reversibility test of MAO-B inhibition by **MK6** or **MK12** after preincubation with the enzyme for 30 min at ∼2 × IC_{50} (i.e., 6.0 nM), as previously described.[44,45] For reference compounds, MAO-B was preincubated with lazabemide (a reference reversible MAO-B inhibitor) or pargyline (a reference irreversible MAO-B inhibitor) at 0.22 and 0.28 μM, respectively. Reversibility patterns were determined by comparing the activities of dialyzed (A_D) and undialyzed (A_U) samples.

Cytotoxicity and ROS Assays. The cytotoxicities and ROS quenching abilities of the lead compounds were evaluated as previously described.[46,47]

Computational Methodology. Detailed procedures for enzyme refining, ligand preparation, molecular docking, and dynamic simulations are described in the Supporting Information.

■ ASSOCIATED CONTENT

Supporting Information

The Supporting Information is available free of charge at https://pubs.acs.org/doi/10.1021/acsomega.2c00397.

^{1}H NMR, ^{13}C NMR, and mass spectra of **MK1** to **MK15** and computational methodology (PDF)

https://doi.org/10.1021/acsomega.2c00397
ACS Omega 2022, 7, 8184−8197

AUTHOR INFORMATION

Corresponding Authors

Bijo Mathew − *Department of Pharmaceutical Chemistry, Amrita School of Pharmacy, Amrita Vishwa Vidyapeetham, Kochi 682041, India*; Email: bijomathew@aims.amrita.edu, bijovilaventgu@gmail.com

Hoon Kim − *Department of Pharmacy, and Research Institute of Life Pharmaceutical Sciences, Sunchon National University, Suncheon 57922, Republic of Korea*; orcid.org/0000-0002-7203-3712; Email: hoon@sunchon.ac.kr

Authors

Jong Min Oh − *Department of Pharmacy, and Research Institute of Life Pharmaceutical Sciences, Sunchon National University, Suncheon 57922, Republic of Korea*

Mohamed A. Abdelgawad − *Department of Pharmaceutical Chemistry, College of Pharmacy, Jouf University, Sakaka, Al Jouf 72341, Saudi Arabia*

Ahmed Khames − *Department of Pharmaceutics and Industrial Pharmacy, College of Pharmacy, Taif University, Taif 21944, Saudi Arabia*

Mohammed M. Ghoneim − *Department of Pharmacy Practice, Faculty of Pharmacy, AlMaarefa University, Ad Diriyah 13713, Saudi Arabia*

Sunil Kumar − *Department of Pharmaceutical Chemistry, Amrita School of Pharmacy, Amrita Vishwa Vidyapeetham, Kochi 682041, India*

Lekshmi R. Nath − *Department of Pharmacognosy, Amrita School of Pharmacy, Amrita Vishwa Vidyapeetham, Kochi 682041, India*

Sachithra Thazhathuveedu Sudevan − *Department of Pharmaceutical Chemistry, Amrita School of Pharmacy, Amrita Vishwa Vidyapeetham, Kochi 682041, India*

Della Grace Thomas Parambi − *Department of Pharmaceutical Chemistry, College of Pharmacy, Jouf University, Sakaka, Al Jouf 72341, Saudi Arabia*

Clement Agoni − *Molecular Bio-Computation and Drug Design Laboratory, School of Health Sciences, University of KwaZulu-Natal, Durban 4001, South Africa*

Mahmoud E. S. Soliman − *Molecular Bio-Computation and Drug Design Laboratory, School of Health Sciences, University of KwaZulu-Natal, Durban 4001, South Africa*; orcid.org/0000-0002-8711-7783

Complete contact information is available at: https://pubs.acs.org/10.1021/acsomega.2c00397

Author Contributions

[▽]B.M. and J.M.O. contributed equally.

Funding

This research was supported by a grant from the Amrita Vishwa Vidyapeetham University (seed grant number K-PHAR-20-628) to B.M.

Notes

The authors declare no competing financial interest.

The models used for MD simulations were prepared using UCSF Chimera (https://www.cgl.ucsf.edu/chimera/). The AutoDock Vina used for molecular docking is available for free download for academic users (https://vina.scripps.edu/). The MD simulations in this study were carried out using the AMBER 18 (https://ambermd.org/). Simulations were analyzed using the CPPTRAJ (https://amber-md.github.io/cpptraj/CPPTRAJ.xhtml), and visualization of structures was performed using the freely available version of Discovery Studio (https://discover.3ds.com/discovery-studio-visualizer-download).

ACKNOWLEDGMENTS

The authors acknowledge the Taif University Researchers Supporting Project (number TURSP-2020/68), Taif University, Taif, Saudi Arabia. The authors also thank the Researchers Supporting Program (number TUMA-Project-2021-6), Al-Maarefa University, Riyadh, Saudi Arabia.

REFERENCES

(1) Tipton, K. F. 90 years of monoamine oxidase: some progress and some confusion. *J. Neural Transm.* **2018**, *125*, 1519−1551.

(2) Tripathi, R. K. P.; Ayyannan, S. R. Monoamine oxidase-B inhibitors as potential neurotherapeutic agents: An overview and update. *Med. Res. Rev.* **2019**, *39*, 1603−1706.

(3) Manzoor, S.; Hoda, N. A comprehensive review of monoamine oxidase inhibitors as Anti-Alzheimer's disease agents: A review. *Eur. J. Med. Chem.* **2020**, *206*, 112787.

(4) Guglielmi, P.; Carradori, S.; Ammazzalorso, A.; Secci, D. Novel approaches to the discovery of selective human monoamine oxidase-B inhibitors: Is there room for improvement? *Expert Opin. Drug Discovery* **2019**, *14*, 995−1035.

(5) Mathew, B.; Parambi, D. G. T.; Mathew, G. E.; Uddin, M. S.; Inasu, S. T.; Kim, H.; Marathakam, A.; Unnikrishnan, M. K.; Carradori, S. Emerging therapeutic potentials of dual-acting MAO and AChE inhibitors in Alzheimer's and Parkinson's diseases. *Arch. Pharm.* **2019**, *352*, No. e1900177.

(6) Zhuang, C.; Zhang, W.; Sheng, C.; Zhang, W.; Xing, C.; Miao, Z. Chalcone: A privileged structure in medicinal chemistry. *Chem. Rev.* **2017**, *117*, 7762−7810.

(7) Guglielmi, P.; Mathew, B.; Secci, D.; Carradori, S. Chalcones: Unearthing their therapeutic possibility as monoamine oxidase B inhibitors. *Eur. J. Med. Chem.* **2020**, *205*, 112650.

(8) Minders, C.; Petzer, J. P.; Petzer, A.; Lourens, A. C. U. Monoamine oxidase inhibitory activities of heterocyclic chalcones. *Bioorg. Med. Chem. Lett.* **2015**, *25*, 5270−5276.

(9) Iacovino, L. G.; Pinzi, L.; Facchetti, G.; Bortolini, B.; Christodoulou, M. S.; Binda, C.; Rastelli, G.; Rimoldi, I.; Passarella, D.; Di Paolo, M. L.; Dalla Via, L. Promising non-cytotoxic monosubstituted chalcones to target monoamine oxidase-B. *ACS Med. Chem. Lett.* **2021**, *12*, 1151−1158.

(10) Hammuda, A.; Shalaby, R.; Rovida, S.; Edmondson, D. E.; Binda, C.; Khalil, A. Design and synthesis of novel chalcones as potent selective monoamine oxidase-B inhibitors. *Eur. J. Med. Chem.* **2016**, *114*, 162−169.

(11) Rehuman, N. A.; Oh, J. M.; Nath, L. R.; Khames, A.; Abdelgawad, M. A.; Gambacorta, N.; Nicolotti, O.; Jat, R. K.; Kim, H.; Mathew, B. Halogenated coumarin-chalcones as multifunctional monoamine oxidase-B and butyrylcholinesterase inhibitors. *ACS Omega* **2021**, *6*, 28182−28193.

(12) Helguera, A.; Perez-Machado, G.; Cordeiro, M. D. S.; Borges, F. Discovery of MAO-B inhibitors—present status and future directions part I: oxygen heterocycles and analogs. *Mini-Rev. Med. Chem.* **2012**, *12*, 907−919.

(13) Tian, C.; Qiang, X.; Song, Q.; Cao, Z.; Ye, C.; He, Y.; Deng, Y.; Zhang, L. Flurbiprofen-chalcone hybrid Mannich base derivatives as balanced multifunctional agents against Alzheimer's disease: Design, synthesis and biological evaluation. *Bioorg. Chem.* **2020**, *94*, 103477.

(14) Sang, Z.; Song, Q.; Cao, Z.; Deng, Y.; Tan, Z.; Zhang, L. Design, synthesis and evaluation of novel dimethylamino chalcone-O-alkylamines derivatives as potential multifunctional agents against Alzheimer's disease. *Eur. J. Med. Chem.* **2021**, *216*, 113310.

(15) Kamecki, F.; Knez, D.; Carvalho, D.; Marcucci, C.; Rademacher, M.; Higgs, J.; Žakelj, S.; Marcos, A.; de Tezanos

Pinto, F.; Abin-Carriquiry, J. A.; Gobec, S.; Colettis, N.; Marder, M. Multitarget 2′-hydroxychalcones as potential drugs for the treatment of neurodegenerative disorders and their comorbidities. *Neuropharmacology* **2021**, *201*, 108837.
(16) Desideri, N.; Fioravanti, R.; Proietti Monaco, L.; Biava, M.; Yáñez, M.; Ortuso, F.; Alcaro, S. 1,5-Diphenylpenta-2,4-dien-1-ones as potent and selective monoamine oxidase-B inhibitors. *Eur. J. Med. Chem.* **2013**, *59*, 91−100.
(17) Suresh, J.; Baek, S. C.; Ramakrishnan, S. P.; Kim, H.; Mathew, B. Discovery of potent and reversible MAO-B inhibitors as furanochalcones. *Int. J. Biol. Macromol.* **2018**, *108*, 660−664.
(18) Maliyakkal, N.; Eom, B. H.; Heo, J. H.; Abdullah Almoyad, M. A.; Thomas Parambi, D. G.; Gambacorta, N.; Nicolotti, O.; Beeran, A. A.; Kim, H.; Mathew, B. A New potent and selective monoamine oxidase-B inhibitor with extended conjugation in a chalcone framework: 1-[4-(Morpholin-4-yl)phenyl]-5-phenylpenta-2,4-dien-1-one. *ChemMedChem* **2020**, *15*, 1629−1633.
(19) Mathew, B.; Carradori, S.; Guglielmi, P.; Uddin, M. S.; Kim, H. New aspects of monoamine oxidase B inhibitors: The key role of halogens to open the golden door. *Curr. Med. Chem.* **2021**, *28*, 266−283.
(20) Lane, R. M.; Potkin, S. G.; Enz, A. Targeting acetylcholinesterase and butyrylcholinesterase in dementia. *Int. J. Neuropsychopharmacol.* **2006**, *9*, 101−124.
(21) Ghosh, A. K.; Osswald, H. L. BACE1 (*β*-secretase) inhibitors for the treatment of Alzheimer's disease. *Chem. Soc. Rev.* **2014**, *43*, 6765−6813.
(22) Cao, Z.; Song, Q.; Yu, G.; Liu, Z.; Cong, S.; Tan, Z.; Deng, Y. Novel 3-benzylidene/benzylphthalide mannich base derivatives as potential multifunctional agents for the treatment of Alzheimer's disease. *Bioorg. Med. Chem.* **2021**, *35*, 116074.
(23) Sellitepe, H. E.; Oh, J. M.; Doğan, İ. S.; Yildirim, S.; Aksel, A. B.; Jeong, G. S.; Khames, A.; Abdelgawad, M. A.; Gambacorta, N.; Nicolotti, O.; Mathew, B.; Kim, H. Synthesis of N′-(4-/3-/2-/Non-substituted benzylidene)-4-[(4-methylphenyl)sulfonyloxy] Benzohydrazides and Evaluation of Their Inhibitory Activities against Monoamine Oxidases and *β*-Secretase. *Appl. Sci.* **2021**, *11*, 5830.
(24) Vishal, V. P.; Oh, J. M.; Khames, A.; Abdelgawad, M. A.; Nair, A. S.; Nath, L. R.; Gambacorta, N.; Ciriaco, F.; Nicolotti, O.; Kim, H.; Mathew, B. Trimethoxylated halogenated chalcones as dual Inhibitors of MAO-B and BACE-1 for the treatment of neurodegenerative disorders. *Pharmaceutics* **2021**, *13*, 850.
(25) Singh, A.; Kukreti, R.; Saso, L.; Kukreti, S. Oxidative stress: A key modulator in neurodegenerative diseases. *Molecules* **2019**, *24*, 1583.
(26) Cournia, Z.; Allen, B.; Sherman, W. Relative binding free energy calculations in drug discovery: Recent advances and practical considerations. *J. Chem. Inf. Model.* **2017**, *57*, 2911−2937.
(27) Wang, C.; Greene, D. A.; Xiao, L.; Qi, R.; Luo, R. Recent developments and applications of the MMPBSA method. *Front. Mol. Biosci.* **2018**, *4*, 87.
(28) Appiah-Kubi, P.; Soliman, M. E. S. Dual anti-inflammatory and selective inhibition mechanism of leukotriene A4 hydrolase/aminopeptidase: insights from comparative molecular dynamics and binding free energy analyses. *J. Biomol. Struct. Dyn.* **2016**, *34*, 2418−2433.
(29) Frimurer, T. M.; Peters, G. H.; Iversen, L. F.; Andersen, H. S.; Møller, N. P. H.; Olsen, O. H. Ligand-induced conformational changes: improved predictions of ligand binding conformations and affinities. *Biophys. J.* **2003**, *84*, 2273−2281.
(30) Teilum, K.; Olsen, J. G.; Kragelund, B. B. Protein stability, flexibility and function. *Biochim. Biophys. Acta* **2011**, *1814*, 969−976.
(31) Karshikoff, A.; Nilsson, L.; Ladenstein, R. Rigidity versus flexibility: the dilemma of understanding protein thermal stability. *FEBS J.* **2015**, *282*, 3899−3917.
(32) Pitera, J. W. Expected distributions of root-mean-square positional deviations in proteins. *J. Phys. Chem. B* **2014**, *118*, 6526−6530.
(33) Bornot, A.; Etchebest, C.; de Brevern, A. G. Predicting protein flexibility through the prediction of local structures. *Proteins* **2011**, *79*, 839−852.
(34) Ali, S.; Hassan, M.; Islam, A.; Ahmad, F. A review of methods available to estimate solvent-accessible surface areas of soluble proteins in the folded and unfolded states. *Curr. Protein Pept. Sci.* **2014**, *15*, 456−476.
(35) Mazal, H.; Aviram, H.; Riven, I.; Haran, G. Effect of ligand binding on a protein with a complex folding landscape. *Phys. Chem. Chem. Phys.* **2018**, *20*, 3054−3062.
(36) Compiani, M.; Capriotti, E. Computational and theoretical methods for protein folding. *Biochemistry* **2013**, *52*, 8601−8624.
(37) Bhattacharyya, A.; Makhal, S. C.; Guchhait, N. Comparative photophysical study of differently substituted cinnamaldehyde-based chalcones: From intramolecular charge transfer to fluorogenic solvent selectivity. *J. Phys. Chem. A* **2019**, *123*, 6411−6419.
(38) Venkidath, A.; Oh, J. M.; Dev, S.; Amin, E.; Rasheed, S. P.; Vengamthodi, A.; Gambacorta, N.; Khames, A.; Abdelgawad, M. A.; George, G.; Nicolotti, O.; Kim, H.; Mathew, B. Selected class of enamides bearing nitro functionality as dual-acting with highly selective monoamine oxidase-B and BACE1 inhibitors. *Molecules* **2021**, *26*, 6004.
(39) Lee, J. P.; Kang, M.-G.; Lee, J. Y.; Oh, J. M.; Baek, S. C.; Leem, H. H.; Park, D.; Cho, M.-L.; Kim, H. Potent inhibition of acetylcholinesterase by sargachromanol I from *Sargassum siliquastrum* and by selected natural compounds. *Bioorg. Chem.* **2019**, *89*, 103043.
(40) Çeçen, M.; Oh, J. M.; Özdemir, Z.; Büyüktuncel, S. E.; Uysal, M.; Mohamed, A. A.; Musa, A.; Gambacorta, N.; Nicolotti, O.; Mathew, B.; Kim, H. Design, synthesis, and biological evaluation of pyridazinones containing the (2-fluorophenyl) piperazine moiety as selective MAO-B inhibitors. *Molecules* **2020**, *25*, 5371.
(41) Heo, J. H.; Eom, B. H.; Ryu, H. W.; Kang, M.-G.; Park, J. E.; Kim, D.-Y.; Kim, J.-H.; Park, D.; Oh, S.-R.; Kim, H. Acetylcholinesterase and butyrylcholinesterase inhibitory activities of khellactone coumarin derivatives isolated from *Peucedanum japonicum* Thurnberg. *Sci. Rep.* **2020**, *10*, 21695.
(42) Jeong, G. S.; Kang, M.-G.; Lee, J. Y.; Lee, S. R.; Park, D.; Cho, M.; Kim, H. Inhibition of butyrylcholinesterase and human monoamine oxidase-B by the coumarin glycyrol and liquiritigenin isolated from Glycyrrhiza uralensis. *Molecules* **2020**, *25*, 3896.
(43) Jeong, G.-S.; Kang, M.-G.; Han, S.-A.; Noh, J.-I.; Park, J.-E.; Nam, S.-J.; Park, D.; Yee, S.-T.; Kim, H. Selective Inhibition of Human Monoamine Oxidase B by 5-hydroxy-2-methyl-chroman-4-one Isolated from an Endogenous Lichen Fungus Daldinia fissa. *J. Fungi* **2021**, *7*, 84.
(44) Lee, H. W.; Ryu, H. W.; Kang, M.-G.; Park, D.; Oh, S.-R.; Kim, H. Potent selective monoamine oxidase B inhibition by maackiain, a pterocarpan from the roots of Sophora flavescens. *Bioorg. Med. Chem. Lett.* **2016**, *26*, 4714−4719.
(45) Baek, S. C.; Lee, H. W.; Ryu, H. W.; Kang, M.-G.; Park, D.; Kim, S. H.; Cho, M.-L.; Oh, S.-R.; Kim, H. Selective inhibition of monoamine oxidase A by hispidol. *Bioorg. Med. Chem. Lett.* **2018**, *28*, 584−588.
(46) Park, C.; Cha, H.-J.; Hong, S. H.; Kim, G.-Y.; Kim, S.; Kim, H.-S.; Kim, B. W.; Jeon, Y.-J.; Choi, Y. H. Protective effect of phloroglucinol on oxidative stress-induced DNA damage and apoptosis through activation of the Nrf2/HO-1 signaling pathway in HaCaT human keratinocytes. *Mar. Drugs* **2019**, *17*, 225.
(47) Pérez, W. I.; Soto, Y.; Ortíz, C.; Matta, J.; Meléndez, E. Ferrocenes as potential chemotherapeutic drugs: Synthesis, cytotoxic activity, reactive oxygen species production and micronucleus assay. *Bioorg. Med. Chem.* **2015**, *23*, 471−479.

https://doi.org/10.1021/acsomega.2c00397
ACS Omega 2022, 7, 8184−8197